Mobius3D

THE COMPLETE PATIENT QA SYSTEM

- **3D PATIENT PLAN QA**
- **3D IMRT/VMAT PRE TREATMENT QA**
- **3D *IN VIVO* DAILY TREATMENT QA**
- **ONLINE PATIENT POSITIONING QA**

Upgrade your patient safety by bridging the gap between patient QA and machine QA:

DoseLab, the complete TG-142 solution, is now integrated into Mobius3D!

Visit mobiusmed.com/mobius3d to learn more or register for a bi-weekly webinar at mobiusmed.com/webinars

MOBIUS MEDICAL SYSTEMS
INNOVATIVE SOFTWARE FOR MODERN RADIATION ONCOLOGY

Low dose interpolated average CT for thoracic PET/CT attenuation correction using an active breathing controller

Tao Sun
Biomedical Imaging Laboratory, Department of Electrical and Computer Engineering, Faculty of Science and Technology, University of Macau, Macau SAR, China

Tung-Hsin Wu
Department of Biomedical Imaging and Radiological Sciences, National Yang Ming University, Taipei 112, Taiwan

Shyh-Jen Wang
Department of Nuclear Medicine, Taipei Veterans General Hospital, Taipei 112, Taiwan

Bang-Hung Yang and Nien-Yun Wu
Department of Biomedical Imaging and Radiological Sciences, National Yang Ming University, Taipei 112, Taiwan and Department of Nuclear Medicine, Taipei Veterans General Hospital, Taipei 112, Taiwan

Greta S. P. Mok[a)]
Biomedical Imaging Laboratory, Department of Electrical and Computer Engineering, Faculty of Science and Technology, University of Macau, Macau SAR, China

(Received 1 June 2013; revised 24 August 2013; accepted for publication 27 August 2013; published 16 September 2013)

Purpose: The temporal mismatch between PET and standard helical CT (HCT) causes substantial respiratory artifacts in PET reconstructed images when using HCT as the attenuation map. Previously we developed an interpolated average CT (IACT) method for attenuation correction (AC) and demonstrated its merits in simulations. In this study we aim to apply IACT in patients with thoracic lesions using an active breathing controller (ABC).
Methods: Under local ethics approval, we recruited 15 patients with a total of 18 lesions in different thoracic regions: left upper lobe (2), right upper lobe (4), right hilum (3), right lower lobe (3), left hilum (2), and esophagus (4). All patients underwent whole body PET scans 1 h after 300–480 MBq ^{18}F-FDG injection, depending on the patients' weight. The PET sinograms were reconstructed with AC using: (i) standard HCT [120 kV, smart mA (30–150 mA), 0.984:1 pitch] and (ii) IACT obtained from end-inspiration and end-expiration breath-hold HCTs (120 kV, 10 mA, 0.984:1 pitch) aided by ABC. IACT was obtained by averaging the intensity of two extreme phases and the interpolated phases between them, where the nonlinear interpolation was obtained by B-spline registration and with an empirical sinusoidal function. The SUV_{max}, SUV_{mean}, and the differences of centroid-of-lesion (d) between PET and different CT schemes were measured for each lesion.
Results: From visual inspection, the respiratory artifacts and blurring generally reduced in the thoracic region for PET_{IACT}. Matching between CT and PET improved for PET_{IACT}, with an average decrease of d for 1.34 ± 1.79 mm as compared to PET_{HCT}. The SUV_{max} and SUV_{mean} were consistently higher for PET_{IACT} versus PET_{HCT} for all lesions, with (30.95 ± 18.63)% and (22.39 ± 15.91)% average increase, respectively.
Conclusions: IACT-ABC reduces respiratory artifacts, PET/CT misregistration and enhances lesion quantitation. This technique is a robust and low dose AC protocol for clinical oncology application especially in the thoracic region. [http://dx.doi.org/10.1118/1.4820976]

Key words: PET/CT, attenuation correction, respiratory artifacts, active breathing controller

1. INTRODUCTION

Image quality of the combined PET/CT is hampered by respiratory misalignments and artifacts. In principle, CT captures a distinct respiratory phase of the thoracic cavity, which does not match with the time-averaged position of the thoracic structures as PET acquisition captures. The problem of respiratory artifacts has been most closely studied for myocardial perfusion PET/CT, while more than 40% of the studies have artifactual defects in the cardiac region when no steps are taken to address the PET/CT alignment, causing significant diagnostic error.[1] Different types of mismatch led to artifacts and increases in myocardial nonuniformity.[2,3] Misregistration of the stress PET/CT also affected the global and regional myocardial blood flow estimation.[4,5] In some studies, underestimation of the standardized uptake value (SUV) of the lung lesions was observed.[6–8] Mismatched attenuation correction (AC) can also cause SUV overestimation for lower lung tumors that are located close to the liver dome, leading to complicated SUV errors.[9] All these PET/CT mismatching

artifacts will lead to inaccurate localization and quantification of tumors, hence potential misdiagnoses.[10–13]

Besides simple manual or automatic registration based on the outline of the heart for the misaligned PET and CT as suggested by Martinez-Möller *et al.*,[4] several methods have been investigated mostly to reduce the PET/CT misalignments and artifacts so far: breathing instruction, CT protocols, and gated four-dimensional (4D) PET/CT. Breathing instruction methods like normal end-expiration breath-hold during the CT scan reduce the occurrence and the severity of respiratory curvilinear artifacts on co-registered PET/CT images,[14] Juan *et al.* showed that PET reconstructed images from patients of normal end-expiration breath-hold group had 28% less incidence rate of artifacts as compared with those from the free-breathing group.[15] This method is not practical for all patients since it requires patients' compliance and may not be feasible for patients with limited pulmonary function.[16] Specific CT protocols based on the axial or helical mode have also been proposed for AC in PET images. Low-pitch CT approximates the average respiratory position and may introduce some blurriness which matches the conditions that occur during the PET measurement.[17] Cine average CT (CACT) was developed for AC in PET and showed significantly less misalignments and artifacts as compared with conventional helical CT (HCT) based AC.[18,19] Alessio *et al.* further evaluated both average and intensity maximum images of 4D CT and indicated the later method had better alignments between PET and CT.[20] The main problem of CACT is relatively high radiation dose. Gated 4D PET/CT provides possible motion compensation in PET reconstruction and motion information for radiation therapy.[21] In 4D PET/CT, each respiratory PET bin can be transformed to a reference target frame that corresponds well to a matched HCT or a CT frame acquired from 4D CT data. All registered bins were used to form a single PET bin for AC to improve quantitative accuracy.[22–25] Recently Fayad *et al.* proposed to generate a virtual 4D CT based on one reference CT image and 4D motion fields obtained from PET to reduce the radiation dose.[26] Liu *et al.* developed another quiescent period gating method to utilize the end-expiration quiescent phase of PET data to match the end-expiration CT.[27] Some investigators incorporated motion estimation into the iterative reconstruction process to lower image noise of gated PET bins which had less photon counts.[28,29] However, its main disadvantages are the high dose from the potential 4D CT, increased acquisition and postprocessing time. More details on different respiratory artifact reduction techniques are described in our previous review.[30]

Formerly we developed an interpolated average CT (IACT) method for AC to reduce PET/CT misalignments. For IACT, two HCTs of the end-inspiration and end-expiration phases are acquired, while interpolated phases are obtained between these two phases using deformable image registration and empirical sinusoidal functions. The IACT is then generated by averaging the original and interpolated phases. Its preliminary effectiveness and possible image quality improvement were evaluated using CACT data in a clinical study,[31] where actual realization was still pending. We then performed a simulation study to evaluate the accuracy and robustness of IACT for different respiratory motion amplitudes and when misplacement occurred for capturing the two extreme phases.[32] In this study, we demonstrate a clinical implementation of IACT with the aid of an active breathing controller (ABC) prototype, and investigate its potential improvement for AC as compared to the conventional HCT in patients with thoracic lesions.

2. MATERIALS AND METHODS

2.A. Patient population

Between October 2012 and December 2012, we recruited 15 patients with a total of 18 lesions in different thoracic regions: left upper lobe (2), right upper lobe (4), right hilum (3), right lower lobe (3), left hilum (2), and esophagus (4). A summary of their demographic data is shown in Table I. This study was approved by the Institutional Review Board of Taipei Veterans General Hospital, and written informed consent was obtained from all patients. All patients were recruited through their scheduled whole-body PET/CT procedures, and those who were with history of inferior pulmonary function or were unable to follow the breath-hold procedures were excluded from this study (n = 3).

2.B. Acquisition protocol

Patients were injected with 300–480 MBq of ^{18}F-FDG, the relative dose measured according to each patient's weight and scanned 1 h postinjection. For each patient, four imaging sessions were acquired:

(i) standard shallow free breathing whole-body HCT [120 kV, smart mA (range 30–150 mA), helical mode, 0.984:1 pitch, 0.5 s gantry rotation];

TABLE I. Patient demographic data.

Patient no.	Sex	Age (yr)	Lesion location	Lesion volume (c.c.)
1	F	65	Left upper lobe	5.29
2	F	66	Right upper lobe	8.28
3	M	86	Right middle lobe, close to rib	3.45
4	M	81	Right middle lobe	21.64
5	M	59	Left upper lobe	7.63
6	M	51	Right upper lobe	2.15
			Right lower lobe	4.54
			Left upper lobe, close to rib	1.3
7	M	59	Right middle lobe	1.45
			Left hilum	5.56
8	M	66	Right hilum	1.6
9	M	72	Right upper lobe	7.09
10	M	88	Right upper lobe, close to rib	9.53
11	M	68	Right middle lobe	11.39
12	M	61	Esophagus	29.6
13	M	47	Esophagus	25.38
14	M	42	Esophagus	4.79
15	M	60	Esophagus	15.48

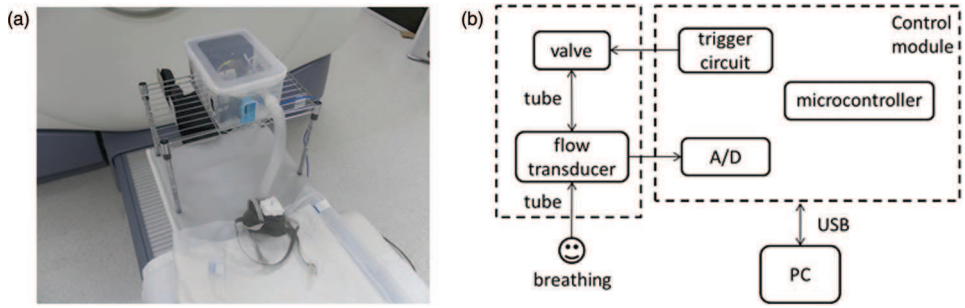

FIG. 1. (a) Overview and (b) block diagram of the ABC system for IACT AC in PET/CT.

(ii) whole-body PET for seven bed positions with 3 min/bed;
(iii) end-inspiration and end-expiration breath-hold HCTs aided with ABC (120 kV, 10 mA helical mode, 0.984:1 pitch, 0.5 s gantry rotation time and a total of 4.4 s/scan) for the thoracic region;
(iv) thoracic PET for two bed positions with 3 min/bed.

All scans were acquired using a PET/CT scanner (Discovery VCT, GE Medical Systems, Milwaukee, WI) in three-dimensional (3D) mode with transaxial field-of-views (FOVs) of 70 and 50 cm for PET and CT, respectively. The thoracic PET was performed due to the fact that the patients changed position after the whole body session for accommodating the ABC device.

2.C. Active breathing controller design

Voluntary breath-hold of end-expiration and end-inspiration phases performed by the patients themselves probably could not represent the normal breathing state as that found in PET acquisition. Using these phases to generate IACT may introduce even more artifacts as compared to conventional HCT. Thus, a noninvasive ABC system (Fig. 1) was developed in this study based on the idea originally proposed by Wong *et al.* for radiotherapy[33] but with certain modifications for PET/CT. It integrates a spirometer, an air mask, and a tube-valve system. Patients were asked to perform mouth-breathing using the air mask that connected to the tube. The flow sensor inserted in the tube detected the real-time breathing flow rate of the patients and sampled the signal to the microcontroller, which further preprocessed the signal and sent it to the PC through a USB connector. An acquisition program based on C++ was developed to process the input signal and control the switching of the valve in the tube. The program can detect the change of the air flow direction according to the flow rate measurement to locate the end-inspiration and end-expiration phases, while the trigger circuit can then automatically control the closing of the valve located in the end of tube to suspend the patients' breathing. Hence, the operator only needs to notify the program when he/she is ready to acquire the CT data.

The flow rates signal can be integrated to determine the change of lung volume during the respiratory cycle. Before the acquisition a system calibration was performed in order to compensate the signal drift caused by the substantial change of temperature and atmospheric pressure. Subjects were coached before the actual CT scans to adapt to the ABC. The operator manually started the HCT scans once the patient had demonstrated the ability to hold his/her breath for ~6 s during the two extreme phases. Sample changes of lung volume during the breathing cycles under the ABC control are shown in Fig. 2.

2.D. IACT generation

B-spline, a deformable image registration algorithm, was applied to calculate the deformation vectors which includes lateral, anterior–posterior, and inferior–superior displacement for each voxel on two CT volumes, i.e., end-inspiration and end-expiration phases obtained from ABC,[34] based on the Insight Segmentation and Registration Toolkit (ITK).[35] One CT image was chosen as the fixed image, i.e., end-inspiration phase, while the other was used as the moving image, i.e., end-expiration phase. A single rigid registration was conducted in the first step. Three stages of B-spline registration were performed later using a multiresolution method in the second step. The grid resolution of the control points improved and their grid-spacing decreased along different stages in this step. The deformation field was determined when the mean square error of the two CT images was smaller than a positive value ε (0.001) in each resolution level.

The forward deformation vector Φ_{ie} was calculated from end-inspiration phase #1 to end-expiration phase #7 and the backward deformation vector Φ_{ei} was calculated from phase #7 to phase #1. For interpolation of Φ_{ie} and Φ_{ei} to obtain the interpolated phases, a diaphragmatic movement function during respiratory cycles was introduced:[36]

$$z(t) = z_0 - b\cos^{2n}\left(\frac{\pi t}{\tau}\right), \tag{1}$$

where $z(t)$ = position of diaphragm at time t, z_0 = diaphragm position at end-expiration, b = amplitude of motion, τ = period of motion, and n = degree of asymmetry which depends on the patient-specific respiratory signals. The power of "2n" made Eq. (1) resulted in more phases near the end-expiration than near the end-inspiration. The inspiration/expiration ratios were calculated for one respiratory cycle for different integer n from Eq. (1) and compared with the actual ratios measured in the acquired breathing signal from each patient, and n was

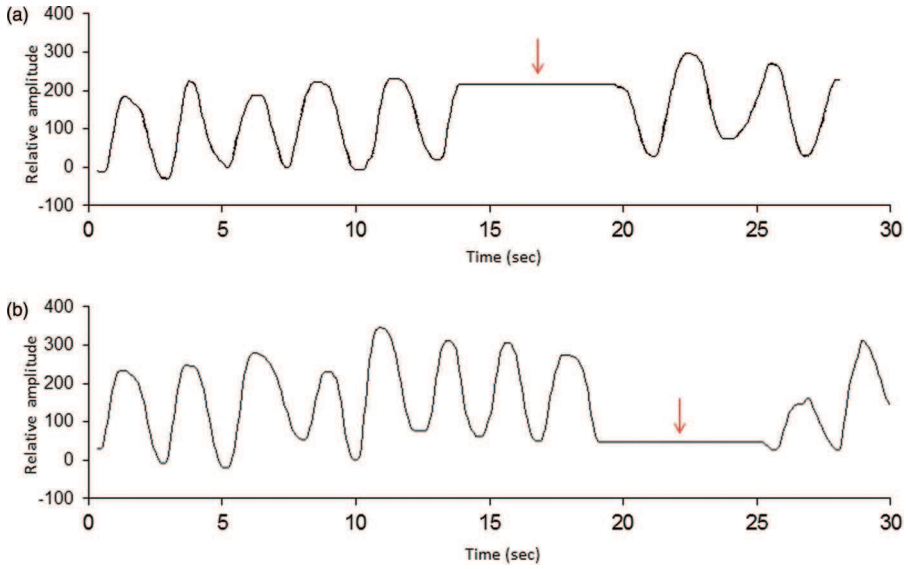

FIG. 2. Change of the respiratory signals during the externally mediated (a) end-inspiration and (b) end-expiration breath-hold controlled by ABC. Red arrows indicated the closing period of the valve.

determined when its corresponding ratios had the best fit with the measured data. In our study, n = 3 was used for most patients except n = 2 for patient #7 and n = 4 for patient #12. To generate intermediate images, Φ_{ie} was divided based on $z(t)$ to obtain interpolated deformation fields. Thus, we can generate interpolated phases #2, #3, #4, #5, and #6 by warping original phase #1 based on Φ_{ie} (Fig. 3). Similarly, phases #8, #9, #10, #11, and #12 were warped from phase #7 based on Φ_{ei}. The final IACT was generated by averaging the image intensity of ten interpolated and two original extreme phases, i.e., a total of 12 phases.

2.E. Data postprocessing and image analysis

The PET raw data were reconstructed using 3D ordered-subset expectation maximization (OS-EM) (28 subsets; 2 iterations; pixel matrix of 128 × 128) algorithm available on the PET/CT workstation. The PET sinograms were corrected for random, scatter, isotope decay and attenuation using HCT and IACT, respectively.

The PET reconstructed images with AC using HCT and IACT, i.e., PET_{HCT} and PET_{IACT}, were registered with associated CT for further analysis.

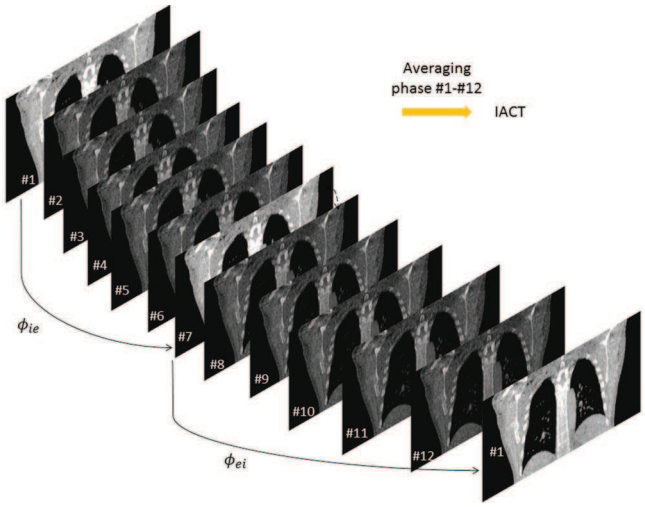

FIG. 3. The deformation fields (Φ_{ie} and Φ_{ei}) obtained from B-spline method were used to generate the interpolated images for IACT based on the empirical sinusoidal function.

2.E.1. Misalignments between PET and CT

A 3D volume-of-interest (VOI) was delineated for each lesion on PET images using a semiautomatic region growing method with a 50% cut off threshold of the maximum intensity value.[37–39] The corresponding delineation for VOI in the CT images was performed with the "lung" window by a radiation oncologist. The coordinates of the centroid of the lesion in PET_{HCT}, HCT, PET_{IACT}, and IACT were determined on the chosen VOIs.[40,41] The distances (d) between the lesion centroid of PET and associate CT were then obtained.

2.E.2. SUV

For each lesion, maximum SUV value (SUV_{max}) and mean SUV value (SUV_{mean}) were measured based on the VOIs drawn on the PET_{HCT} and PET_{IACT} images.

2.E.3. Radiation dose

For different CT protocols and subjects, the radiation dose was expressed using the effective dose in mSv for the thoracic region. An approximation of the effective dose was obtained by multiplying the volume CT dose length product (mGy-cm) as reported by the manufacturer's software with a conversion factor k (0.014 mSv mGy^{-1} cm^{-1}).[42]

TABLE II. Summary of different quantitative figures-of-merit for HCT and IACT AC methods.

	SUV_{max}			SUV_{mean}			*d* (mm)		
Patient no.	PET_{HCT}	PET_{IACT}	%diff	PET_{HCT}	PET_{IACT}	%diff	HCT/PET_{HCT}	$IACT/PET_{IACT}$	Diff. (mm)
1	5.98	7.01	17.22	2.48	2.78	12.1	6.28	5.91	− 0.37
2	7.99	9.07	13.52	3.89	5.81	49.36	3.79	6.49	2.7
3	4.64	6.26	33.84	2.89	2.98	3.11	6.6	4.67	− 1.93
4	12.03	14.97	24.44	4.96	5.75	15.93	4.68	4.59	− 0.09
5	3.27	5.67	73.39	1.23	1.8	46.34	7.32	6.22	− 1.1
6	6.39	7.91	23.79	3.77	4.83	28.12	4.74	1.97	− 2.77
	2.47	2.67	8.1	1.32	1.52	15.15	6.58	4.47	− 2.11
	3.5	4.35	24.29	2.22	2.77	24.77	13.77	8.79	− 4.98
7	1.98	2.77	39.9	1.2	1.91	59.17	5.27	4.39	− 0.88
	2.69	3.29	20.07	1.51	1.53	1.32	12.12	14.67	2.55
8	1.53	2.35	53.59	1.01	1.11	9.9	6.55	6.47	− 0.08
9	7.84	8.46	7.91	3.96	4.57	15.4	2.93	0.57	− 2.36
10	1.84	2.83	53.8	1.47	1.92	30.61	4.91	5.53	0.62
11	7.65	10.71	40	5.32	6.75	26.88	9.34	1.36	− 7.98
12	15.77	21.3	35.07	9.3	11.75	26.34			
13	4.77	4.98	4.4	3.23	3.66	15.48	N/A (Lesions cannot be delineated on CT images)		
14	8.12	10.85	33.62	5.21	5.77	10.75			
15	6.27	9.41	50.08	3.69	4.14	12.2			
Mean	5.82	7.49	30.95	3.26	3.96	22.39	6.78	5.44	− 1.34
SD	1.94	2.21	18.63	1.45	1.62	15.91	3.07	3.46	2.79

3. RESULTS

For all 15 patients with 18 lesions, IACT generally reduced lesion mismatch (*d*) between CT and corresponding PET attenuation corrected images (Table II), with average decrease of 1.34 ± 1.79 mm among all measurable lesions. The centroid difference was not obtainable for patients with esophageal lesions as they could not be delineated on the CT images.

Meanwhile, the SUV_{max} and SUV_{mean} for the lesions are summarized in Table II. PET_{IACT} generally showed increased SUV_{max} and SUV_{mean} for all lesions when compared to PET_{HCT}. The percentage increments (%diff) are (30.95 ± 18.63)% and (22.39 ± 15.91)% for SUV_{max} and SUV_{mean}, respectively.

Sample images of three patients with lung lesions are shown in Fig. 4–6, respectively. In Fig. 4, the IACT AC method provided a better matching for the CT and PET image as compared to HCT for AC. The visual assessment matched with the quantitative measurement of the centroid difference between CT and PET in Table II ($d_{HCT/PET\text{-}HCT}$ = 9.34 mm; $d_{IACT/PET\text{-}IACT}$ = 1.36 mm; diff = −7.98 mm). For another patient as demonstrated in Fig. 5, the contrast of the lesion in the right upper lobe substantially improved for PET_{IACT} as compared to $PET_{HCT,}$ with increase of SUV_{max} and SUV_{mean} of 53.8% and 30.61%, respectively. The general resolution also improved for PET_{IACT} as compared to PET_{HCT} in this patient as indicated in the vertical profiles drawn on Fig. 5(c), where the lesion full-width-at-half-maximum appeared to be smaller with improved structure details in the liver region on PET_{IACT}. The PET_{HCT} had severe "cold" artifacts around the left ventricle region and also in the region close to the left diaphragm, while the artifacts reduced in the PET_{IACT}. Characteristic curvilinear artifact was also observed on PET_{HCT} in patient #13 (Fig. 6).

The estimated effective dose was 0.38 mSv for IACT for the thoracic region, while HCT had an average effective dose

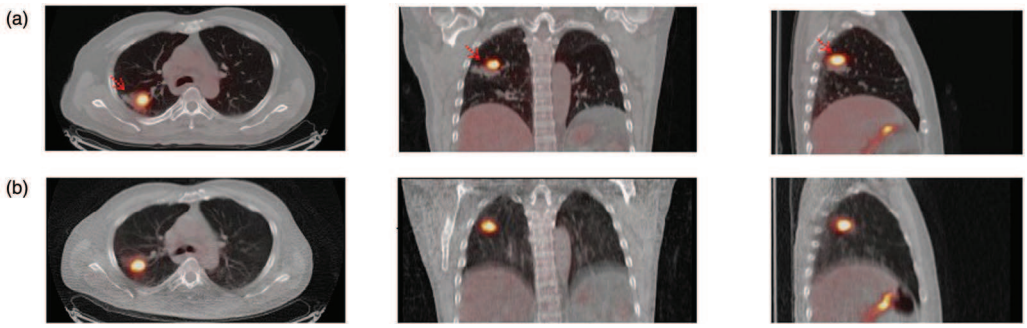

FIG. 4. Transaxial (left), coronal (middle), and sagittal (right) views of the fused PET/CT images for (a) HCT- and (b) IACT-AC for patient #11. Red arrows indicated a lesion in the right upper lobe of the lung.

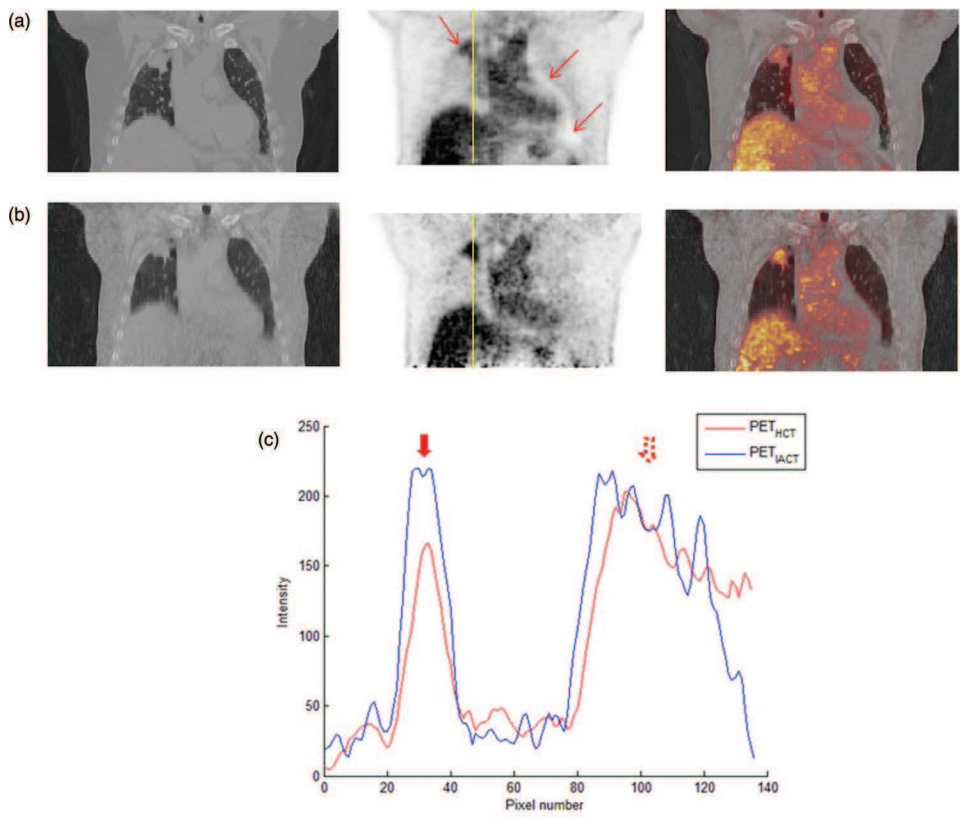

FIG. 5. Sample coronal images of (a) HCT (left); PET_{HCT} (middle); fusion image (right) and (b) IACT (left); PET_{IACT} (middle); fusion image (right) for patient #10. Artifacts around the left diaphragm and left ventricle region were observed on the PET_{HCT} images (red arrows). (c) Vertical image profiles drawn across the lesion on PET_{HCT} and PET_{IACT} images. Red arrow indicated the lesion area and the dotted red arrow indicated the liver region.

of 2.1 mSv (1.58–2.42 mSv) in the same region. The IACT reduced up to 84.29% effective dose as compared to HCT method in this study.

4. DISCUSSION

Our ABC device samples the respiratory signal by detecting the air flow with 20 Hz sampling frequency, while the peaks and the valleys of the signal indicates end-inspiration and end-expiration phases, respectively. During the acquisition, the operator observes the real time signal and indicates when he/she is ready for acquiring the CT data. The acquisition program will then automatically determine the extreme phases and send a high level voltage signal to the electronic board to close the valve connected to the breathing tube with <0.1 s. The patient will hear a sharp sound from the closing valve and a backward force from the tube will then enforce the patient to hold his/her breath. The time from the valve closing to patient's response lasts <1 s. We thus set the valve closing time to ∼6 s to enable patients to hold their breath sufficiently long enough for the HCT scan, which takes ∼4.4 s. The short breath-holding time particularly enhances the feasibility of this study, as compared with other breathing-instruction methods.[40] Our former simulation study showed that the IACT generated from the "shifted" respiratory phases, i.e., the phases right after the extreme phases, provided very similar results of the IACT generated from the exact end-inspiration and end-expiration phases. Besides, some patients may have residual breathing after the valve is closed (Fig. 7), which may affect the subsequent IACT generation. Thus, besides coaching, all patients underwent a mock

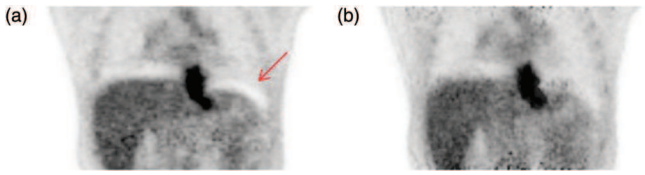

FIG. 6. Coronal views of (a) PET_{HCT} and (b) PET_{IACT} for patient #13. Curvilinear artifact was observed on PET_{HCT} (red arrow) but reduced on PET_{IACT}.

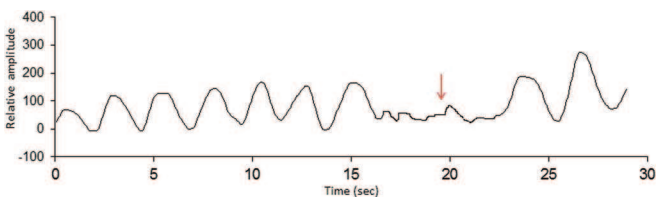

FIG. 7. Sample respiratory signal of a patient indicated residual breathing (red arrow) during a breath hold mediated by the ABC.

acquisition before the experiment to confirm their compliance of breath-holding.

We used tube current of 10 mA for the IACT acquisition because it was the lowest value available on the current scanner. Even though the 10 mA CT images are much nosier than the conventional diagnostic CT studies, they are still feasible for generating the IACT for AC in PET/CT. While IACT only imposed 0.38 mSv dose from two separate low dose HCT scans to each patient, the improvement of image quality and quantitative accuracy was substantial. According to Xia *et al.*,[43] the PET noise introduced by the ultralow dose CT scans does not significantly affect the diagnostic information and the image quality of the associate attenuation-corrected PET. Hence, CT dose can be reduced while it is mainly for AC and providing registered anatomical information, but may not be feasible for diagnostic purpose. Notably, the IACT for PET AC is relatively smoothed by averaging the extreme and interpolated images. Thus, extra smoothing for CT raw data was not performed before the IACT generation.

The movement of the structures in the thorax is highly correlated to the diaphragm motion during the respiration.[44] Thus, in this paper, we utilized a diaphragmatic movement function [Eq. (1)] during the respiratory cycles to model the lesion movement pattern. On the other hand, the B-spline method used in this study estimated the deformation vector of the lesion in three directions: superior-to-inferior, anterior-to-posterior, and lateral. However, this combined vector may not indicate hysteresis motion when the lesion moving trajectories are not consistent from inspiration to expiration and vice versa. This motion will induce a larger tumor volume size appeared in the PET images as compared to its real size, leading to the PET/CT misalignment. The lesions in the upper lung are more subject to the respiratory hysteresis and are more complicated to model as compared to the ones in the lower lung.[45,46] In this study, we observed that only some of the lesions in the upper lung had inferior mismatching in IACT-AC than using HCT-AC (patient #2). The motion is even more complex with the lesions attached to the rigid structure in the thorax, e.g., the pleura near the ribcage (patient #10). So far, we did not observe significant difference in terms of the quantification results for different thoracic regions which may due to the number of lesions in each region was still low. However, the preliminary results from our simulation showed that the improvement from IACT was more obvious for the lesions in the lower lung. The effects of the lesion sizes, locations, uptake ratios and movement pattern on IACT effectiveness are being further investigated in our current simulation study. We are also recruiting more subjects and developing a better categorization scheme to improve the statistics in each region.

Patients tend to spend more time towards the end-expiration period[9] and this can be reflected in the asymmetry of the respiratory signal. For each patient, this degree of asymmetry was represented by an integer n in Eq. (1) and can be determined for each patient specifically according to their acquired respiratory signal by calculating the elapsed time ratio between expiration and inspiration. Thus, our sinusoidal function for interpolation is indeed semipatient specific. One may suggest using the fully patient specific breathing signal for the interpolation function. However, our preliminary study showed that the quantitative difference of the PET results of using these two functions were negligible. Also, the errors of determination of the PET and CT centroids were negligible, with ~1% and ~3% for CT and PET, respectively, for a 6 mm spherical lesion with 8:1 uptake ratio from our simulation study (data not shown).

One major concern in this study is that the PET_{IACT} was done after the PET_{HCT}, due to the positioning of the ABC device was not feasible for the standard whole-body PET protocol. Thus, concatenating the IACT into the standard whole-body HCT (Ref. 19) was not a possible option in this study. The longer activity distribution time for thoracic PET acquisition may "artificially" enhance the lesion SUV (Ref. 47) and overestimate the effectiveness of IACT. However, we found the average SUV_{mean} increase (32.9%) of the malignant lung tumors ($n = 9$) was substantially higher than the increased value (20.5%) as suggested by Matthies *et al.* who evaluated dual time point FDG PET for pulmonary nodules,[48] even the delay between 2nd and 1st PET scan was just 30 min as compared to ~60 min in other dual time point studies. Also, all benign lung lesions ($n = 5$) in this study showed obvious SUV increase in PET_{IACT} as compared to PET_{HCT}, although they usually do not demonstrate increased SUV for dual time point scans.[48] The lesion centroid differences between PET and associate CT also confirmed the effectiveness of IACT (Table II). In the future study, we will implement an improved protocol so that the thoracic IACT can be incorporated into the standard whole-body HCT directly to become a composite whole-body CT dataset for whole-body PET reconstruction[19] to rule out the potential delayed uptake effect. Besides, the IACT generation is automatically done with two registration processes, while gated 4D PET/CT may require multiple registrations. For CACT, there is no external respiratory monitoring device and breath-hold required for the acquisition, making it clinically more favorable. However, the dose reduction of IACT as compared to CACT is still substantial (0.38 mSv vs less than 1 mSv,[13] 1.35 mSv,[19] and 2.36 mSv[1]). We have also applied the IACT for PET/CT cardiac scans and showed substantial image quality improvement on the reconstructed images.[49]

5. CONCLUSION

In this study, we have developed an ABC prototype and evaluated the clinical feasibility of IACT-ABC method on patients with thoracic tumors. We showed that it potentially improved PET reconstructed image quality as compared to the conventional HCT, with reduced respiratory artifacts and spatial mismatch, increased SUV of the lesions and lowered radiation dose. IACT with the aid of ABC is a robust method for thoracic PET/CT AC and is promising to improve diagnostic accuracy.

ACKNOWLEDGMENTS

The authors would like to thank the staff of National PET and Cyclotron Center in Taipei Veterans General Hospital for

their clinical and technical assistance. The authors would also like to thank Dr. George Watt from the Department of English of University of Macau for proofreading the paper. This work was supported in parts by the Multi-Year Research Grant Nos. (MYRG185(Y3-L3)-FST11-MSP and MYRG077(Y2-L2)-FST12-MSP) of University of Macau, Macau and the research grant (NSC 99-2314-B-010-043-MY3) from National Science Council, Taiwan. The authors declare that they have no conflict of interest.

[a]Author to whom correspondence should be addressed. Electronic mail: gretamok@umac.mo; Telephone: (853) 8397-8465.

[1]K. L. Gould, T. Pan, C. Loghin, N. P. Johnson, A. Guha, and S. Sdringola, "Frequent diagnostic errors in cardiac PET/CT due to misregistration of CT attenuation and emission PET images: A definitive analysis of causes, consequences, and corrections," J. Nucl. Med. **48**(7), 1112–1121 (2007).

[2]S. McQuaid and B. Hutton, "Sources of attenuation-correction artefacts in cardiac PET/CT and SPECT/CT," Eur. J. Nucl. Med. Mol. Imaging **35**(6), 1117–1123 (2008).

[3]C. Loghin, S. Sdringola, and K. L. Gould, "Common artifacts in PET myocardial perfusion images due to attenuation–emission misregistration: Clinical significance, causes, and solutions," J. Nucl. Med. **45**(6), 1029–1039 (2004).

[4]A. Martinez-Möller, M. Souvatzoglou, N. Navab, M. Schwaiger, and S. G. Nekolla, "Artifacts from misaligned CT in cardiac perfusion PET/CT studies: Frequency, effects, and potential solutions," J. Nucl. Med. **48**(2), 188–193 (2007).

[5]M. Rajaram, A. K. Tahari, A. H. Lee, M. A. Lodge, B. Tsui, S. Nekolla, R. L. Wahl, F. M. Bengel, and P. E. Bravo, "Cardiac PET/CT misregistration causes significant changes in estimated myocardial blood flow," J. Nucl. Med. **54**(1), 50–54 (2013).

[6]Y. E. Erdi, S. A. Nehmeh, T. Pan, A. Pevsner, K. E. Rosenzweig, G. Mageras, E. D. Yorke, H. Schoder, W. Hsiao, O. D. Squire, P. Vernon, J. B. Ashman, H. Mostafavi, S. M. Larson, and J. L. Humm, "The CT motion quantitation of lung lesions and its impact on PET-measured SUVs," J. Nucl. Med. **45**(8), 1287–1292 (2004).

[7]S. A. Nehmeh and Y. E. Erdi, "Respiratory motion in positron emission tomography/computed tomography: A review,"Semin. Nucl. Med. **38**(3), 167–176 (2008).

[8]M. C. Adams, T. G. Turkington, J. M. Wilson, and T. Z. Wong, "A systematic review of the factors affecting accuracy of SUV measurements," Am. J. Roentgenol. **195**(2), 310–320 (2010).

[9]C. Liu, L. A. Pierce II, A. M. Alessio, and P. E. Kinahan, "The impact of respiratory motion on tumor quantification and delineation in static PET/CT imaging," Phys. Med. Biol. **54**(24), 7345–7362 (2009).

[10]M. M. Osman, C. Cohade, Y. Nakamoto, and R. L. Wahl, "Respiratory motion artifacts on PET emission images obtained using CT attenuation correction on PET-CT," Eur. J. Nucl. Med. Mol. Imaging **30**(4), 603–606 (2003).

[11]M. Allen-Auerbach, K. Yeom, J. Park, M. Phelps, and J. Czernin, "Standard PET/CT of the chest during shallow breathing is inadequate for comprehensive staging of lung cancer," J. Nucl. Med. **47**(2), 298–301 (2006).

[12]G. K. von Schulthess, H. C. Steinert, and T. F. Hany, "Integrated PET/CT: Current applications and future directions," Radiology **238**(2), 405–422 (2006).

[13]T. Pan and H. Zaidi, "Attenuation correction strategies for positron emission tomography/computed tomography and 4-dimensional positron emission tomography/computed tomography," PET Clin. **8**(1), 37–50 (2013).

[14]G. W. Goerres, E. Kamel, B. Seifert, C. Burger, A. Buck, T. F. Hany, and G. K. von Schulthess, "Accuracy of image coregistration of pulmonary lesions in patients with non-small cell lung cancer using an integrated PET/CT system," J. Nucl. Med. **43**(11), 1469–1475 (2002).

[15]R. de Juan, B. Seifert, T. Berthold, G. K. von Schulthess, and G. W. Goerres, "Clinical evaluation of a breathing protocol for PET/CT," Eur. Radiol. **14**(6), 1118–1123 (2004).

[16]S. Senan, D. De Ruysscher, P. Giraud, R. Mirimanoff, and V. Budach, "Literature-based recommendations for treatment planning and execution in high-dose radiotherapy for lung cancer," Radiother. Oncol. **71**(2), 139–146 (2004).

[17]J. A. Nye, F. Esteves, and J. R. Votaw, "Minimizing artifacts resulting from respiratory and cardiac motion by optimization of the transmission scan in cardiac PET/CT," Med. Phys. **34**(6), 1901–1906 (2007).

[18]T. Pan, O. Mawlawi, S. A. Nehmeh, Y. E. Erdi, D. Luo, H. H. Liu, R. Castillo, R. Mohan, Z. Liao, and H. A. Macapinlac, "Attenuation correction of PET images with respiration-averaged CT images in PET/CT," J. Nucl. Med. **46**(9), 1481–1487 (2005).

[19]T. Pan, O. Mawlawi, D. Luo, H. H. Liu, P.-C. M. Chi, M. V. Mar, G. Gladish, M. Truong, J. Jeremy Erasmus, Z. Liao, and H. A. Macapinlac, "Attenuation correction of PET cardiac data with low-dose average CT in PET/CT," Med. Phys. **33**(10), 3931–3938 (2006).

[20]A. M. Alessio, S. Kohlmyer, K. Branch, G. Chen, J. Caldwell, and P. Kinahan, "Cine CT for attenuation correction in cardiac PET/CT," J. Nucl. Med. **48**(5), 794–801 (2007).

[21]S. A. Nehmeh, Y. E. Erdi, T. Pan, A. Pevsner, K. E. Rosenzweig, E. Yorke, G. S. Mageras, H. Schoder, P. Vernon, O. Squire, H. Mostafavi, S. M. Larson, and J. L. Humm, "Four-dimensional (4D) PET/CT imaging of the thorax," Med. Phys. **31**(12), 3179–3186 (2004).

[22]C. C. A. Nagel, G. Bosmans, A. L. A. J. Dekker, M. C. Ollers, D. K. M. D. Ruysscher, P. Lambin, A. W. H. Minken, N. Lang, and K. P. Schafers, "Phased attenuation correction in respiration correlated computed tomography/positron emitted tomography," Med. Phys. **33**(6), 1840–1847 (2006).

[23]R. G. Wells, T. D. Ruddy, R. A. DeKemp, J. N. DaSilva, and R. S. Beanlands, "Single-phase CT aligned to gated PET for respiratory motion correction in cardiac PET/CT," J. Nucl. Med. **51**(8), 1182–1190 (2010).

[24]S. J. McQuaid, T. Lambrou, and B. F. Hutton, "A novel method for incorporating respiratory-matched attenuation correction in the motion correction of cardiac PET–CT studies," Phys. Med. Biol. **56**(10), 2903–2915 (2011).

[25]D. Didierlaurent, S. Ribes, H. Batatia, C. Jaudet, L. O. Dierickx, S. Zerdoud, S. Brillouet, O. Caselles, and F. Courbon, "The retrospective binning method improves the consistency of phase binning in respiratory-gated PET/CT," Phys. Med. Biol. **57**(23), 7829–7841 (2012).

[26]H. J. Fayad, F. Lamare, C. C. Le Rest, V. Bettinardi, and D. Visvikis, "Generation of 4-dimensional CT images based on 4-dimensional PET–derived motion fields," J. Nucl. Med. **54**(4), 631–638 (2013).

[27]C. Liu, A. Alessio, L. Pierce, K. Thielemans, S. Wollenweber, A. Ganin, and P. Kinahan, "Quiescent period respiratory gating for PET/CT," Med. Phys. **37**(9), 5037–5043 (2010).

[28]F. Lamare, M. J. L. Carbayo, T. Cresson, G. Kontaxakis, A. Santos, C. C. L. Rest, A. J. Reader, and D. Visvikis, "List-mode-based reconstruction for respiratory motion correction in PET using non-rigid body transformations," Phys. Med. Biol. **52**(17), 5187–5204 (2007).

[29]N. Grotus, A. J. Reader, S. Stute, J. C. Rosenwald, P. Giraud, and I. Buvat, "Fully 4D list-mode reconstruction applied to respiratory-gated PET scans," Phys. Med. Biol. **54**(6), 1705–1721 (2009).

[30]T. Sun and G. S. P. Mok, "Techniques for respiration-induced artifacts reductions in thoracic PET/CT," Quant. Imaging Med. Surg. **2**, 46–52 (2012).

[31]T.-C. Huang, G. S. P. Mok, S.-J. Wang, T.-H. Wu, and G. Zhang, "Attenuation correction of PET images with interpolated average CT for thoracic tumors," Phys. Med. Biol. **56**(8), 2559–2567 (2011).

[32]G. S. P. Mok, S. Tao, H. Tzung-Chi, and M. I. Vai, "Interpolated average CT for attenuation correction in PET - A simulation study," IEEE Trans. Bio-Med. Eng. **60**(7), 1927–1934 (2013).

[33]J. W. Wong, M. B. Sharpe, D. A. Jaffray, V. R. Kini, J. M. Robertson, J. S. Stromberg, and A. A. Martinez, "The use of active breathing control (ABC) to reduce margin for breathing motion," Int. J. Radiat. Oncol. Biol. Phys. **44**(4), 911–919 (1999).

[34]D. Sarrut, V. Boldea, S. Miguet, and C. Ginestet, "Simulation of four-dimensional CT images from deformable registration between inhale and exhale breath-hold CT scans," Med. Phys. **33**(3), 605–617 (2006).

[35]T. S. Yoo, M. J. Ackerman, W. E. Lorensen, W. Schroeder, V. Chalana, S. Aylward, D. Metaxas, and R. Whitaker, "Engineering and algorithm design for an image processing Api: A technical report on ITK – The Insight Toolkit," Stud. Health Technol. Inform. **85**, 586–592 (2002).

[36]A. E. Lujan, J. M. Balter, and R. K. T. Haken, "A method for incorporating organ motion due to breathing into 3D dose calculations in the liver: Sensitivity to variations in motion," Med. Phys. **30**(10), 2643–2649 (2003).

[37]R. Boellaard, M. O'Doherty, W. Weber, F. Mottaghy, M. Lonsdale, S. Stroobants, W. G. Oyen, J. Kotzerke, O. Hoekstra, J. Pruim, P. Marsden, K. Tatsch, C. Hoekstra, E. Visser, B. Arends, F. Verzijlbergen, J. Zijlstra, E. I. Comans, A. Lammertsma, A. Paans, A. Willemsen, T. Beyer, A.

Bockisch, C. Schaefer-Prokop, D. Delbeke, R. Baum, A. Chiti, and B. Krause, "FDG PET and PET/CT: EANM procedure guidelines for tumour PET imaging: Version 1.0," Eur. J. Nucl. Med. Mol. Imaging **37**(1), 181–200 (2010).

[38]K. Mah, C. B. Caldwell, Y. C. Ung, C. E. Danjoux, J. M. Balogh, S. N. Ganguli, L. E. Ehrlich, and R. Tirona, "The impact of 18 FDG-PET on target and critical organs in CT-based treatment planning of patients with poorly defined non-small-cell lung carcinoma: A prospective study," Int. J. Radiat. Oncol. Biol. Phys. **52**(2), 339–350 (2002).

[39]E. Deniaud-Alexandre, E. Touboul, D. Lerouge, D. Grahek, J.-N. Foulquier, Y. Petegnief, B. Grès, H. El Balaa, K. Keraudy, K. Kerrou, F. Montravers, B. Milleron, B. Lebeau, and J.-N. Talbot, "Impact of computed tomography and 18F-deoxyglucose coincidence detection emission tomography image fusion for optimization of conformal radiotherapy in non–small-cell lung cancer," Int. J. Radiat. Oncol. Biol. Phys. **63**(5), 1432–1441 (2005).

[40]S. A. Nehmeh, Y. E. Erdi, G. S. P. Meirelles, O. Squire, S. M. Larson, J. L. Humm, and H. Schöder, "Deep-inspiration breath-hold PET/CT of the thorax," J. Nucl. Med. **48**(1), 22–26 (2007).

[41]L. Fin, J. Daouk, J. Morvan, P. Bailly, I. Esper, L. Saidi, and M.-E. Meyer, "Initial clinical results for breath-hold CT-based processing of respiratory-gated PET acquisitions," Eur. J. Nucl. Med. Mol. Imaging **35**(11), 1971–1980 (2008).

[42]G. Bongartz, S. J. Golding, A. G. Jurik, M. Leonardi, E. van Persijn van Meerten, R. Rodríguez, K. Schneider, A. Calzado, J. Geleijns, K. A. Jessen, W. Panzer, P. C. Shrimpton, and G. Tosi, *European Guidelines for Multislice Computed Tomography* (European Commission, Brussels, Belgium, 2004).

[43]T. Xia, A. M. Alessio, B. De Man, R. Manjeshwar, E. Asma, and P. E. Kinahan, "Ultra-low dose CT attenuation correction for PET/CT," Phys. Med. Biol. **57**(2), 309–328 (2012).

[44]L. I. Cervino, A. K. Chao, A. Sandhu, and S. B. Jiang, "The diaphragm as an anatomic surrogate for lung tumor motion," Phys. Med. Biol. **54**(11), 3529–3541 (2009).

[45]Y. Seppenwoolde, H. Shirato, K. Kitamura, S. Shimizu, M. van Herk, J. V. Lebesque, and K. Miyasaka, "Precise and real-time measurement of 3D tumor motion in lung due to breathing and heartbeat, measured during radiotherapy," Int. J. Radiat. Oncol. Biol. Phys. **53**(4), 822–834 (2002).

[46]V. Boldea, G. C. Sharp, S. B. Jiang, and D. Sarrut, "4D-CT lung motion estimation with deformable registration: Quantification of motion nonlinearity and hysteresis," Med. Phys. **35**(3), 1008–1018 (2008).

[47]S. Basu, H. Zaidi, S. Holm, and A. Alavi, "Quantitative techniques in PET-CT imaging," Curr. Med. Imaging Rev. **7**(3), 216–233 (2011).

[48]A. Matthies, M. Hickeson, A. Cuchiara, and A. Alavi, "Dual time point 18F-FDG PET for the evaluation of pulmonary nodules," J. Nucl. Med. **43**(7), 871–875 (2002).

[49]T.-H. Wu, G. Zhang, S.-J. Wang, C.-H. Chen, B.-H. Yang, N.-Y. Wu, and T.-C. Huang, "Low-dose interpolated average CT for attenuation correction in cardiac PET/CT," Nucl. Instrum. Meth. A **619**(1–3), 361–364 (2010).